

# Application of the density dependent hadron field theory to neutron star matter

F. Hofmann, C. M. Keil, H. Lenske

*Institut für Theoretische Physik, Universität Gießen, Heinrich-Buff-Ring 16, 35392 Gießen,  
Germany*

(October 28, 2018)

## Abstract

The density dependent hadron field (DDRH) theory, previously applied to isospin nuclei and hypernuclei is used to describe  $\beta$ -stable matter and neutron stars under consideration of the complete baryon octet. The meson-hyperon vertices are derived from Dirac-Brueckner calculations of nuclear matter and extended to hyperons. We examine properties of density dependent interactions derived from the Bonn A and from the Groningen NN potential as well as phenomenological interactions. The consistent treatment of the density dependence introduces rearrangement terms in the expression for the baryon chemical potential. This leads to a more complex condition for the  $\beta$ -equilibrium compared to standard relativistic mean field (RMF) approaches. We find a strong dependence of the equation of state and the particle distribution on the choice of the vertex density dependence. Results for neutron star masses and radii are presented. We find a good agreement with other models for the maximum mass. Radii are smaller compared to RMF models and indicate a closer agreement with results of non-relativistic Brueckner calculations.

PACS number(s): 26.60.+c, 21.65.+f, 21.30.Fe, 97.60.Jd

## I. INTRODUCTION

The nuclear equation of state (EoS) is the fundamental input for the calculation of neutron star properties. The internal structure of a neutron star ranges from sub-nuclear densities at the surface to a few times the normal nuclear matter density  $\rho_0$  in its core. Therefore, a detailed knowledge of the EoS over a wide range of densities is required. Of particular importance is the behavior of the EoS for densities  $\rho \gg \rho_0$  since it primarily determines the maximum mass of the star. Comparison with experimentally observed data for neutron star masses and radii might allow us to examine the reliability of different models for the EoS at high densities.

The theoretical determination of such an EoS is a very hard task since there is only accurate knowledge around  $\rho = \rho_0$  where matter in the weak equilibrium consists mainly of nucleons and leptons. At higher densities of  $2 - 3 \rho_0$  one expects strange baryons to appear as new hadronic degrees of freedom. The extrapolation of the EoS to high densities and its implication on neutron star properties has been examined in a variety of models, most notably in the framework of phenomenological non-relativistic potential models [1], relativistic mean-field approaches (RMF) [2–5] and non-relativistic Brueckner-Hartree-Fock (BHF) calculations [6,7]. In addition there have been calculations employing chiral effective Lagrangians [8] or the quark meson coupling model [9]. From a microscopic point of view Brueckner calculations using realistic nucleon-nucleon (NN) and hyperon-nucleon (YN) potentials as input have to be preferred. Since the density inside neutron stars is extremely high - the Fermi momenta and the baryon effective mass are in the order of 500 MeV - the use of non-relativistic models might be problematic and one should prefer a relativistic description. Due to technical difficulties, relativistic (Dirac) BHF calculations are restricted to asymmetric nuclear matter and the inclusion of hyperons at higher densities is at present not feasible. Therefore, only DB calculations for neutron star matter with nucleons have been performed [10,11].

RMF theory [12,13] allows to incorporate easily and consistently an enlarged set of hadronic degrees of freedom and has been successfully applied to hypernuclei [14–17] and neutron stars [2,4,5]. Being a phenomenological model with its parameters usually adjusted to the properties of finite nuclei and their limited density range around  $\rho_0$ , an extrapolation to higher densities has some uncertainties. Parameterizations with an excellent description of finite nuclei turn out to be unstable at higher densities being mainly caused by divergent scalar self-interaction terms [18]. Nucleons acquire negative effective masses and the equation of state turns out to be much stiffer compared to Dirac-Brueckner calculations [5]. One solution is the introduction of a quartic vector self-interaction term [19,20]. Also, calculations in relativistic Hartree-Fock approximation with coupling constants fitted to the EoS of DB calculations were successfully applied to neutron star matter [21,22].

In this paper we employ results from DB calculations by parameterizing the DB self-energies in terms of density dependent coupling functionals and apply them in Hartree approximation to strange and neutron star matter. This approach, the density dependent hadron field (DDRH) field theory, has been introduced in [23,24] and applied to stable [25–27] and exotic nuclei [28]. Taking into account information from realistic NN potentials and a much wider density range ( $0.5 - 3 \rho_0$ ) we expect our extrapolation to high densities to be more stable than purely phenomenological RMF models.

An important point is the treatment of the hyperons. In the DDRH model they can be treated in almost the same manner as in standard RMF theory, allowing an easy extension of the model to the  $SU(3)_f$  octet baryons as was shown in [29]. Since we assume in general density dependent hyperon-meson vertices we should in principle derive their parameterization from DB calculations that include hyperons. Since such calculations are not available we extrapolate the density dependence and the strength of the vertices from DB calculations of nuclear matter and from hypernuclear data. As discussed in [29] this provides at least qualitative information about DB results of strange matter. This approach is discussed in Sec. II where also a short review of the theoretical model is given. In Sec. III we apply the derived density dependent hyperon-nucleon interaction to  $N\Lambda$  matter and to neutron star matter in  $\beta$ -equilibrium. We discuss the influence of the density dependence on the chemical potential and present results for the equation of state for various density dependent interactions. Neutron star matter compositions for different models are presented. In Sec. IV the influence of the calculated EoS on mass-radius relations of neutron stars is investigated and compared with previous results of other groups. The paper closes in Sec. V with a summary and conclusions.

## II. DENSITY DEPENDENT HADRON FIELD THEORY WITH HYPERONS

### A. The Model Lagrangian

The model Lagrangian closely follows in structure the one of relativistic mean- field (RMF) theory [12,13]. The important difference in the density dependent relativistic hadron field theory (DDRH) corresponds to replacing the constant meson-baryon vertices of the RMF model by functionals  $\hat{\Gamma}(\hat{\rho})$  of Lorenz-scalar bilinear forms  $\hat{\rho}(\bar{\Psi}_F, \Psi_F)$  of the baryon field operators. This step is necessary to retain thermodynamical consistency and energy-momentum conservation for this extended model and has been discussed in detail in [24,25]. In the meson-exchange particle sector we have also included the scalar isovector meson  $\delta$  in contrast to previous formulations since it is expected to be important in very asymmetric systems.

In this work the extension to hypernuclei as introduced in [29] is used. The  $1/2^+$  baryon octet is taken into account including the  $S = -1$  ( $\Lambda, \Sigma$ ) and  $S = -2$  ( $\Xi$ ) hyperons. Besides the standard set of non- strange mesons we also include the hidden-strangeness meson fields  $\sigma_s$  (scalar,  $m_{\sigma_s} = 975$  MeV) and  $\phi$  (vector,  $m_\phi = 1020$  MeV) [30].

Defining the flavour spinor  $\Psi_F$

$$\Psi_F = (\Psi_N, \Psi_\Lambda, \Psi_\Sigma, \Psi_\Xi)^T \quad (1)$$

which is composed of the isospin multiplets

$$\begin{aligned} \Psi_N &= \begin{pmatrix} \psi_p \\ \psi_n \end{pmatrix}, & \Psi_\Lambda &= \psi_\Lambda, \\ \Psi_\Sigma &= \begin{pmatrix} \psi_{\Sigma^+} \\ \psi_{\Sigma^0} \\ \psi_{\Sigma^-} \end{pmatrix}, & \Psi_\Xi &= \begin{pmatrix} \psi_{\Xi^0} \\ \psi_{\Xi^-} \end{pmatrix}, \end{aligned} \quad (2)$$

the Lagrangian is written as

$$\begin{aligned}\mathcal{L} &= \mathcal{L}_B + \mathcal{L}_M + \mathcal{L}_{int} \\ \mathcal{L}_B &= \overline{\Psi}_F \left[ i\gamma_\mu \partial^\mu - \hat{M}_F \right] \Psi_F\end{aligned}\tag{3}$$

$$\begin{aligned}\mathcal{L}_M &= \frac{1}{2} \sum_{i=\sigma,\delta,\sigma_s} \left( \partial_\mu \Phi_i \partial^\mu \Phi_i - m_i^2 \Phi_i^2 \right) - \\ &\quad \frac{1}{2} \sum_{\kappa=\omega,\rho,\phi} \left( \frac{1}{2} F_{\mu\nu}^{(\kappa)} F^{(\kappa)\mu\nu} - m_\kappa^2 A_\mu^{(\kappa)} A^{(\kappa)\mu} \right)\end{aligned}\tag{4}$$

$$\begin{aligned}\mathcal{L}_{int} &= \overline{\Psi}_F \tilde{\Gamma}_\sigma \Psi_F \Phi_\sigma - \overline{\Psi}_F \tilde{\Gamma}_\omega \gamma_\mu \Psi_F A^{(\omega)\mu} + \\ &\quad \overline{\Psi}_F \tilde{\Gamma}_\delta \boldsymbol{\tau} \Psi_F \Phi_\delta - \overline{\Psi}_F \tilde{\Gamma}_\rho \gamma_\mu \boldsymbol{\tau} \Psi_F \mathbf{A}^{(\rho)\mu} + \\ &\quad \overline{\Psi}_F \tilde{\Gamma}_{\sigma_s} \Psi_F \Phi_{\sigma_s} - \overline{\Psi}_F \tilde{\Gamma}_\phi \gamma_\mu \Psi_F A^{(\phi)\mu}.\end{aligned}\tag{5}$$

$\mathcal{L}_B$  and  $\mathcal{L}_M$  are the free baryonic and mesonic Lagrangians, respectively. Baryon-meson interactions are described by  $\mathcal{L}_{int}$  that includes the vertex functionals  $\tilde{\Gamma}(\overline{\Psi}_F, \Psi_F)$ . The diagonal matrix  $\hat{M}$  contains the free-space baryon masses. The Lagrangian and the interaction have to be symmetric in flavor space, since  $SU(3)_f$ -flavor exchanging mesons are not considered. This is obtained by defining the vertices as

$$\left( \tilde{\Gamma}_\alpha \right)_{BB'} = \hat{\Gamma}_{\alpha B} \delta_{BB'}. \tag{6}$$

The indices  $\alpha = \sigma, \omega, \delta, \rho, \sigma_s, \phi$  and  $B = N, \Lambda, \Sigma, \Xi$  denote all mesons and baryon multiplets. The most general *ansatz* for the DDRH vertices, allowing to treat the density dependence of each vertex independently, is

$$\hat{\Gamma}_{\alpha B} \left( \hat{\rho}_{\alpha B}(\overline{\Psi}_F, \Psi_F) \right) \tag{7}$$

where  $\hat{\rho}_{\alpha B}$  is a Lorentz-scalar combination of the baryon field operators. As discussed in the introduction, the strength and the intrinsic density dependence of the vertices have to be deduced from microscopic calculations. The mapping of the DBHF self-energies to infinite nuclear matter DDRH vertices is done in the local density approximation (LDA), e.g. [23,31,32], and has been thoroughly discussed in [28,29]. In [28] a momentum correction of the self-energies was introduced to improve the applicability of DB calculations to the relativistic Hartree approximation. DB self-energies derived in asymmetric nuclear matter [32] were parameterized and special care was taken to reproduce the DB binding energy over the complete asymmetry range from isospin symmetric nuclear matter to pure neutron matter.

The standard choice is to let the density operator  $\hat{\rho}$  depend on the baryon vector current  $\hat{j}_\mu = \overline{\Psi} \gamma_\mu \Psi$ . This so called vector density dependence (VDD) leads to quite satisfactory results for finite nuclei [25] and hypernuclei [29] and is a natural choice for the parameterization of the DB self-energies as was discussed in [28]. A straightforward extension to meson-hyperon vertices is the *ansatz* [29]

$$\hat{\rho}_{\alpha B}[\overline{\Psi}_F, \Psi_F] = \overline{\Psi}_F \tilde{B}_{\alpha B}^\mu \gamma_\mu \Psi_F. \tag{8}$$

Different choices of the matrix  $\tilde{B}_{\alpha B}^\mu$  and their physical significance will be discussed in the next section. Taking the variational derivative of the Lagrangian

$$\frac{\delta \mathcal{L}_{int}}{\delta \bar{\Psi}_F} = \frac{\partial \mathcal{L}_{int}}{\partial \bar{\Psi}_F} + \sum_{\alpha, B} \frac{\partial \mathcal{L}_{int}}{\partial \hat{\rho}_{\alpha B}} \frac{\delta \hat{\rho}_{\alpha B}}{\delta \bar{\Psi}_F}. \quad (9)$$

leads to the usual meson field equations known from RMF theory but replacing the constant couplings  $g_{\alpha B}$  by density dependent vertices  $\hat{\Gamma}_{\alpha B}(\hat{\rho})$ . In the baryon field equations additional rearrangement contributions appear that have their origin in the second term of Eq. (9),

$$[\gamma_\mu (i\partial^\mu - \tilde{\Sigma}^{\mu(0)} - \tilde{\Sigma}^{\mu(r)}) - (\tilde{M} - \tilde{\Sigma}^{s(0)})] \Psi_F = 0. \quad (10)$$

The scalar self-energy  $\tilde{\Sigma}^{s(0)}$  has the standard form, while the vector self-energy  $\tilde{\Sigma}^\mu = \tilde{\Sigma}^{\mu(0)} + \tilde{\Sigma}^{\mu(r)}$  includes rearrangement contributions  $\tilde{\Sigma}^{\mu(r)}$  introduced by the medium-dependence of the vertices.

$$\tilde{\Sigma}^{s(0)} = \tilde{\Gamma}_\sigma \Phi_\sigma + \tilde{\Gamma}_\delta \boldsymbol{\tau} \Phi_\delta + \tilde{\Gamma}_{\sigma_s} \Phi_{\sigma_s} \quad (11)$$

$$\tilde{\Sigma}^{\mu(0)} = \tilde{\Gamma}_\omega A^{(\omega)\mu} + \tilde{\Gamma}_\rho \boldsymbol{\tau} A^{(\rho)\mu} + \tilde{\Gamma}_\phi A^{(\phi)\mu} \quad (12)$$

$$\tilde{\Sigma}^{\mu(r)} = \sum_{\alpha, B} \frac{\partial \mathcal{L}_{int}}{\partial \hat{\rho}_{\alpha B}} \tilde{B}_{\alpha B}^\mu \quad (13)$$

The importance of the rearrangement energies  $\tilde{\Sigma}^{\mu(r)}$  and their physical origin has been discussed in detail in [25,33]. Their explicit form and their impact on neutron star matter will be discussed in the next sections.

## B. Choice of the density dependence

The density dependence of the hyperon-meson vertex functionals should in principle be derived directly from DB self-energies of strange matter performed with the complete baryon octet. However, such a full scale calculation is not available and hardly feasible under present conditions. Non-relativistic Brueckner calculations with microscopic interactions have been performed for strange matter by several groups [34–36] but, obviously, their results can not be used in relativistic calculations because of the different structure of the non-relativistic single particle potentials. Therefore, we choose a semiempirical approach by relating the microscopic density dependence of the meson-nucleon vertices derived from DB calculations of pure isospin matter (only  $p, n$ ) to the density dependence of the hyperon- nucleon and hyperon- hyperon interaction.

In [29] we have shown by inspecting the properties of the Dirac- Brueckner interaction in strange matter that density dependent nucleon and hyperon dynamics can be related to each other to a good approximation by scaling laws. The main outcome is that the hyperon and nucleon self-energies and vertices are related to each other by the ratio of the free space coupling constants  $\bar{g}_{\alpha B}$ . In leading order Hartree approximation one finds the relation

$$R_{\alpha Y} = \frac{\Gamma_{\alpha Y}}{\Gamma_{\alpha N}} \simeq \frac{\Sigma_{\alpha Y}}{\Sigma_{\alpha N}} \simeq \frac{\bar{g}_{\alpha Y}}{\bar{g}_{\alpha N}}. \quad (14)$$

Since this relation is strictly valid only for symmetric hypermatter with the same content of nucleons and hyperons [29] it is not obvious how the density dependence of the hyperon

vertices has to be related to the full baryonic density for other matter compositions. An obvious and rather simple approach is to let all vertices depend on the total baryon density, denoted by  $\hat{\rho}_T$ . From now on we will denote this choice as model 1. For the hyperons this corresponds to defining the coupling functionals as

$$\begin{aligned}\hat{\Gamma}_{\alpha\Lambda} &= R_{\alpha\Lambda}\hat{\Gamma}_{\alpha N}(\hat{\rho}_T), \\ \hat{\Gamma}_{\alpha\Sigma} &= R_{\alpha\Sigma}\hat{\Gamma}_{\alpha N}(\hat{\rho}_T), \\ \hat{\Gamma}_{\alpha\Xi} &= R_{\alpha\Xi}\hat{\Gamma}_{\alpha N}(\hat{\rho}_T).\end{aligned}\quad (15)$$

The parameterization of the density dependence is taken from the nucleon- vertices  $\hat{\Gamma}_{\alpha N}(\hat{\rho}_N)$  derived from DB calculations of nuclear matter where  $\hat{\rho}_N \equiv \hat{\rho}_T$ . By relating the density  $\hat{\rho}_T$  to the total baryon vector current

$$\hat{\rho}_T = \sqrt{\hat{j}_\mu^F \hat{j}^{\mu F}}. \quad (16)$$

a Lorentz-invariant expression is obtained which is equivalent to choosing the matrix  $\tilde{B}_\mu^{\alpha B}$  in Eq. (8) as

$$\tilde{B}_\mu^{\alpha B} \equiv \tilde{B}_\mu = \hat{u}_\mu \text{diag}(1, 1, 1, 1), \quad (17)$$

where  $\hat{u}^\mu$  is a four velocity with  $\hat{u}^\mu \hat{u}_\mu = 1$ . This choice leads to rearrangement self-energies of the form

$$\begin{aligned}\hat{\Sigma}^{\mu(r)} &= \sum_{B'} \left( \frac{\partial \hat{\Gamma}_{\omega B'}}{\partial \hat{\rho}_{B'}} A_\nu^{(\omega)} \hat{j}_{B'}^\nu - \frac{\partial \hat{\Gamma}_{\sigma B'}}{\partial \hat{\rho}_{B'}} \Phi_\sigma \hat{\rho}_{B'}^s \right. \\ &\quad + \frac{\partial \hat{\Gamma}_{\rho B'}}{\partial \hat{\rho}_{B'}} \mathbf{A}_\nu^{(\rho)} \overline{\Psi}_{B'} \gamma^\nu \boldsymbol{\tau} \Psi_{B'} - \frac{\partial \hat{\Gamma}_{\delta B'}}{\partial \hat{\rho}_{B'}} \Phi_\delta \overline{\Psi}_{B'} \boldsymbol{\tau} \Psi_{B'} \\ &\quad \left. + \frac{\partial \hat{\Gamma}_{\phi B'}}{\partial \hat{\rho}_{B'}} A_\nu^{(\phi)} \hat{j}_{B'}^\nu - \frac{\partial \hat{\Gamma}_{\sigma_s B'}}{\partial \hat{\rho}_{B'}} \Phi_{\sigma_s} \hat{\rho}_{B'}^s \right) \hat{u}^\mu\end{aligned}\quad (18)$$

where the scalar densities are defined as  $\hat{\rho}_B^s = \overline{\Psi}_B \Psi_B$ . Since the density dependence of all vertices was chosen to depend on the same argument  $\hat{\rho}_T$  the summation has to be performed over all  $B'$  leading to identical rearrangement self-energies for all baryon multiplets. Also, in a system consisting of different fractions of hyperons and nucleons, the scaling relation for the vertices is fulfilled for all densities and independent of the strangeness fraction.

In Ref. [29]  $\Lambda$ -hypernuclei were considered and the medium modification of the vertices was chosen to depend only on the density of the surrounding baryons of same particle type, e.g.  $\hat{\Gamma}_{\alpha\Lambda}(\hat{\rho}_\Lambda)$ . The parameterization of the density dependence was taken from the nucleon-vertices  $\hat{\Gamma}_{\alpha N}(\hat{\rho}_N)$  derived from DB calculations of nuclear matter. We will denote this choice as model 2. Extending this model to the complete baryon octet, we let the vertices only depend on the density of baryons of the same multiplet

$$\begin{aligned}\hat{\Gamma}_{\alpha\Lambda} &= R_{\alpha\Lambda}\hat{\Gamma}_{\alpha N}(\hat{\rho}_\Lambda), \\ \hat{\Gamma}_{\alpha\Sigma} &= R_{\alpha\Sigma}\hat{\Gamma}_{\alpha N}(\hat{\rho}_\Sigma), \\ \hat{\Gamma}_{\alpha\Xi} &= R_{\alpha\Xi}\hat{\Gamma}_{\alpha N}(\hat{\rho}_\Xi),\end{aligned}\quad (19)$$

where the densities are the baryon vector currents of the corresponding baryon species

$$\hat{\rho}_B = \sqrt{\hat{j}_\mu^B \hat{j}^{\mu B}}. \quad (20)$$

In this model the matrix  $\tilde{B}_\mu^{\alpha B}$  in Eq. (8) is defined as

$$\tilde{B}_\mu^{\alpha B} \equiv \tilde{B}_\mu^B = \hat{u}_\mu \text{diag}(\delta^{NB}, \delta^{\Lambda B}, \delta^{\Sigma B}, \delta^{\Xi B}) \quad (21)$$

and the rearrangement self-energies now differ between the baryon multiplets

$$\begin{aligned} \hat{\Sigma}_B^{\mu(r)} = & \left( \frac{\partial \hat{\Gamma}_{\omega B}}{\partial \hat{\rho}_B} A_\nu^{(\omega)} \hat{j}_B^\nu - \frac{\partial \hat{\Gamma}_{\sigma B}}{\partial \hat{\rho}_B} \Phi_\sigma \hat{\rho}_B^s \right. \\ & + \frac{\partial \hat{\Gamma}_{\rho B}}{\partial \hat{\rho}_B} A_\nu^{(\rho)} \bar{\Psi}_B \gamma^\nu \boldsymbol{\tau} \Psi_B - \frac{\partial \hat{\Gamma}_{\delta B}}{\partial \hat{\rho}_B} \Phi_\delta \bar{\Psi}_B \boldsymbol{\tau} \Psi_B \\ & \left. + \frac{\partial \hat{\Gamma}_{\phi B}}{\partial \hat{\rho}_B} A_\nu^{(\phi)} \hat{j}_B^\nu - \frac{\partial \hat{\Gamma}_{\sigma_s B}}{\partial \hat{\rho}_B} \Phi_{\sigma_s} \hat{\rho}_B^s \right) \hat{u}^\mu. \end{aligned} \quad (22)$$

This separation of the density dependence also corresponds in first order to the outcome of DB considerations and leads to satisfying results for  $\Lambda$ -hypernuclei. It takes into account that in leading order the medium dependence of the vertices is only caused by Pauli-blocked intermediate states of baryons of the same multiplet. On the other hand, this separation leads to a variation of the relative strength of the vertices in strongly asymmetric systems, e.g. neutron stars, since the vertices depend on different arguments  $\hat{\rho}_B$ . This behavior is different compared to standard RMF calculations where the ratio of the vertices stays constant over the whole density range and is independent of the strangeness content.

The two vertex models constitute limiting cases where model 1 (dependence on  $\rho_T$ ) is probably most realistic for systems at high total baryon densities. Model 2 (dependence on  $\rho_B$ ), on the other hand, can be expected to be most realistic for low hyperon densities as found in single  $\Lambda$ -hypernuclei. We assume that a realistic density dependence should be composed as a mixture of the total density and the baryon multiplet density

$$\hat{\Gamma}_{\alpha B} \equiv \hat{\Gamma}_{\alpha B}(\hat{\rho}_B, \hat{\rho}_T) \quad (23)$$

Unfortunately, DB calculations from which such a functional dependence could be extracted are not yet available. Our choice, taking into account both extremes, allows us to examine thoroughly the properties of such a parameterization. Furthermore, for pure systems, consisting only of e.g.  $\Lambda$ , both models are identical.

### C. The vertex scaling factors

In RMF theory the phenomenological hyperon and nucleon vertices can be related to each other by simple scaling factors  $R_{\alpha Y}$ , e.g.  $g_{\alpha \Lambda} = R_{\alpha \Lambda} g_{\alpha N}$ . As shown in Section II B this relation also holds in the DDRH model. A widely used approach is to determine these vertex scaling factors from SU(6) symmetry relations of the quark model [37]. For the vector mesons ideal mixing is assumed and one finds [30]

$$\begin{aligned}\Gamma_{\omega\Lambda} = \Gamma_{\omega\Sigma} = 2\Gamma_{\omega\Xi} &= \frac{2}{3}\Gamma_{\omega N}, \\ \Gamma_{\rho\Sigma} = 2\Gamma_{\rho\Xi} = 2\Gamma_{\rho N}, \quad \Gamma_{\rho\Lambda} &= 0\end{aligned}\tag{24}$$

$$\begin{aligned}2\Gamma_{\phi\Lambda} = 2\Gamma_{\phi\Sigma} = 2\Gamma_{\phi\Xi} &= -\frac{2\sqrt{2}}{3}\Gamma_{\omega N} \\ \Gamma_{\phi N} &= 0.\end{aligned}\tag{25}$$

The scalar coupling constants are fitted to hypernuclear properties [14–16] and chosen to give hyperon potentials in saturated nuclear matter that are compatible with experimental results for the single particle spectra of hypernuclei.

$$U_{\Lambda}^{(N)} = U_{\Sigma}^{(N)} = -30 \text{ MeV}, \quad U_{\Xi}^{(N)} = -28 \text{ MeV}.\tag{26}$$

The values of the  $\Lambda$ ,  $\Sigma$  and  $\Xi$  potentials were chosen in accordance with Ref. [5,30]. Based on the analysis of  $\Sigma^-$  atomic data the real part of the optical potential was found to be negative [38]. A recent analysis, however, indicates that the isoscalar potential changes sign in the nuclear interior and becomes repulsive [39]. Therefore, we also performed calculations with a potential depth of  $U_{\Sigma}^{(N)} = +30$  MeV and found that the  $\Sigma$  does not appear in the composition of neutron star matter. For this reason we restrict our discussion to the negative potential value. The  $\Xi$  nuclear interaction also exhibits large uncertainties with potential depths ranging from  $-14$  MeV to  $-28$  MeV in some investigations [40].

In DDRH theory the non-relativistic single particle potentials of hyperons in nuclear matter are obtained as

$$U_Y^{(N)} = \Sigma_Y^{0(0)} + \Sigma_Y^{0(r)} - \Sigma_Y^{s(0)}.\tag{27}$$

Choosing  $U_Y^{(N)}$  as fixed by phenomenology this relation introduces a constraint on the couplings  $\Gamma_{\sigma Y}$  and  $\Gamma_{\omega Y}$ . Due to the different density dependence of model 1 and 2 one finds different values for the scaling factors  $R_{\sigma Y}$  even though they were adjusted to the same potential depth. In model 1 the hyperon vertices have to be evaluated at saturation density  $\rho_T = \rho_0$  even though the density of the hyperons is  $\rho_Y \ll \rho_T$ . In addition, the rearrangement contributions of the nucleons add to the hyperon potential. In contrast, in model 2 the vertices have to be calculated at vanishing hyperon density and rearrangement does not contribute to the hyperon potential.

We examined the behavior of three different density dependent interactions. The Bonn A parameter set [31] parameterizes the density dependence of DB Brueckner calculations in symmetric nuclear matter with the Bonn A NN potential [41,42]. It only includes density dependent vertices for the  $\sigma$  and the  $\omega$  meson while the  $\rho$  meson coupling strength was chosen as a constant. Calculations for single  $\Lambda$ -hypernuclei have been performed successfully with this parameterization [29]. The Groningen parameter set [28] was fitted to DB Brueckner calculations in asymmetric nuclear matter with the Groningen NN potential [32,43,44]. In addition to the isoscalar channel it includes a density dependence in the isovector part of the interaction, parameterized by the  $\rho$  and the  $\delta$  nucleon-meson vertices. The third parameter set is a phenomenological interaction whose density dependence ( $\sigma$ ,  $\omega$  and  $\rho$  meson) has been adjusted by a fit to nuclear matter properties and finite nuclei [45]. It will be denoted from now on as DD. The quality of its description of finite nuclei is comparable to RMF

parameter sets including nonlinear meson interaction terms and its nuclear matter properties at higher densities are in accordance with DB calculations. Results for the scaling factors are presented in the right column of Tab. I. From now on, the set of scaling factors  $R_{\alpha Y}$  that was determined from the SU(6) symmetry relations of the quark model will be denoted as  $R_q$ .

It is our aim to start from DB theory and use microscopic interactions as input for our calculations. Since these results include highly nonlinear and nonperturbative correlation effects, the strict use of the quark model reduction of  $R_{\omega\Lambda} = 2/3$  might be questionable. Therefore, we examine in addition the properties of microscopically derived scaling factors. For the Bonn A potential an extension to the free  $N\Lambda$  systems exist [46,47], but DB calculations are pending. A free space scalar vertex scaling factor  $R_{\sigma\Lambda} = 0.49$  was extracted from  $N\Lambda$  T-matrix results for a sharp  $\sigma$  meson mass  $m_\sigma = 550$  MeV [47]. Following Eq. (14) we can apply this value also to the in- medium vertices.

Since microscopic values for  $R_{\omega\Lambda}$  are not available from Ref. [47] we use it as a phenomenological parameter and adjust it to the potential depth  $U_\Lambda^{(N)}$ . In this analysis we are restricted to the  $\Lambda$  because calculations for  $N\Sigma$  and  $N\Xi$  systems were not yet performed. For the Bonn A potential we find a value of  $R_{\omega\Lambda} = 0.569$  in model 2 in close agreement with [29] where a value of  $R_{\omega\Lambda} = 0.553$  was found by a fit a  $\Lambda$  single-particle energies. In a constant coupling RMF model [48] a relative  $\omega$  coupling of  $R_{\omega\Lambda} = 0.512$  was found for the same value of  $R_{\sigma\Lambda}$ . This is again in close agreement with our corresponding values of model 1, e.g.  $R_{\omega\Lambda} = 0.510$  for the phenomenological density dependence. Results for the vector meson scaling factors  $R_{\omega\Lambda}$  for model 1 and 2 for the different interactions are shown in the left column of Tab. I. We will denote this set of semi-microscopic scaling factors by  $R_m$ .

In [46,47] the scalar meson channels were described by the correlated exchange of pion and kaon pairs. Therefore, the scalar coupling also includes a relevant admixtures of the  $\sigma_s$  field in the  $\Lambda$  coupling. Adjusting the vector coupling we also implicitly include contributions from the  $\phi$  field. Naive quark counting suggests that even for a pure  $\Lambda$ - $\Lambda$  interaction the strange mesons contribute only about 10% of the interaction strength. For this reason we neglect the explicit contributions from the  $\sigma_s$  and  $\phi$  meson in our calculations. In addition, it should be noted that the contribution from these hidden- strangeness mesons can not be fixed by experimental data, introducing additional ambiguities in the model as seen in [40].

In the next section we will show that there are already notable differences between the different models without these additional fields. The notable deviations of  $R_{\sigma\Lambda}$  and  $R_{\omega\Lambda}$  to the quark model value of 2/3 originate in higher order nonlinear contributions from the dynamically generated  $\sigma$  and  $\sigma_s$  exchange channels [46,47], the explicit  $SU(3)_f$  symmetry breaking and the  $\omega$ -  $\phi$  octet-singlet mixing on the fundamental strong interaction level.

### III. MEAN-FIELD DESCRIPTION OF STRANGE AND $\beta$ -STABLE MATTER

#### A. Properties of strange matter

We now apply the extended DDRH model of Sec. II to  $\Lambda$  matter and  $\beta$ -stable matter. A solvable scheme is obtained in mean-field theory which amounts to taking the expectation values with respect to the Hartree ground state of the baryon-meson vertices and the meson

fields. The vertices then reduce to density dependent functions  $\Gamma_{\alpha B}(\rho)$  of the baryon density  $\rho$ . In static infinite matter all derivative terms vanish and the solution of the fields can be expressed analytically [13].

In weak  $\beta$ -equilibrium electrons  $e^-$  and myons  $\mu^-$  have to be included in the Lagrangian due to the weak decay channel,

$$\Psi_L = (\psi_e, \psi_\mu)^T \quad (28)$$

$$\mathcal{L}_L = \overline{\Psi}_L \left[ i\gamma_\mu \partial^\mu - \tilde{M}_L \right] \Psi_L. \quad (29)$$

In mean-field theory the energy density  $\epsilon$  and the pressure  $P$  are given by the ground state expectation values of the energy-momentum tensor  $T^{\mu\nu}$ . One finds

$$\epsilon = \langle T^{00} \rangle = \sum_{i=b,l} \frac{1}{4} [3E_{F_i}\rho_i + m_i^* \rho_i^s] \quad (30)$$

$$+ \sum_b \frac{1}{2} [\rho_b \Sigma_b^{0(0)} + \rho_b^s \Sigma_b^{s(0)}]$$

$$P = \frac{1}{3} \sum_{i=1}^3 \langle T^{ii} \rangle = \sum_{i=b,l} \frac{1}{4} [E_{F_i}\rho_i - m_i^* \rho_i^s] \quad (31)$$

$$+ \sum_b \frac{1}{2} [\rho_b \Sigma_b^{0(0)} - \rho_b^s \Sigma_b^{s(0)} + 2\rho_b \Sigma_b^{0(r)}]$$

where the indices  $b = p, n, \Lambda, \Sigma^-, \Sigma^0, \Sigma^+, \Xi^-, \Xi^0$  and  $l = e^-, \mu^-$  run over all baryons and leptons, respectively. The self-energies are the mean-field expectation values of the quantities defined in Eqs. (11)-(13),  $E_{F_b} = \sqrt{k_{F_b}^2 + m_b^{*2}}$  is the energy of the particle,  $k_F$  is the Fermi momentum and  $m_b^* = M_b - \Sigma_b^s$  the effective mass.

The chemical potential in a system with fixed baryon number is defined as

$$\mu_b = \frac{\partial \epsilon}{\partial \rho_b} = \sqrt{k_{F_b}^2 + m_b^{*2}} + \Sigma_b^{0(0)} + \Sigma_b^{0(r)} \quad (32)$$

In contrast to constant coupling RMF models the rearrangement energy appears in the above relation which is mandatory for thermodynamical consistency. This can be easily verified by applying the Hugenholtz-van Hove theorem [49] that relates energy and pressure of a particle to its chemical potential and noting that the rearrangement contribution also appears in the expression for the pressure.

In weak  $\beta$ -equilibrium the chemical potentials of all particles are related to each other by

$$\mu_i = b_i \mu_n - q_i \mu_e \quad (33)$$

which imposes charge and baryon number conservation. Here, the index  $i$  denotes all particle species (baryons and leptons) and  $b_i$  and  $q_i$  are the corresponding baryon number and electrical charge. The equilibrium problem is solved by determining the meson fields from the field equations of the form

$$m_\alpha^2 \Phi_\alpha = \sum_b \Gamma_{\alpha b}(\tilde{\rho}) \tilde{\rho}_b \quad (34)$$

where  $\tilde{\rho}$  depends on the choice of model 1 or 2. The densities  $\tilde{\rho}_b$  are the (iso)scalar or (iso)vector densities and are determined by the Lorentz and isospin structure of the corresponding meson vertex. As an additional constraint the total baryon density  $\rho$  is fixed and charge neutrality is imposed for neutron star matter

$$\rho = \sum_i b_i \rho_i, \quad \rho_c = \sum_i q_i \rho_i = 0. \quad (35)$$

This allows the determination of the electron  $\mu_e$  and baryon  $\mu_n$  chemical potentials in  $\beta$ -equilibrium. In contrast to standard RMF calculations one can not simply extract the Fermi momentum  $k_{F_i}$  and thus the density  $\rho_i = k_{F_i}^3 / 3\pi^2$  of each particle for a fixed chemical potential from Eqs. (32) and (33). Since the self-energies depend by virtue of the vertices on the densities of the baryons a coupled set of equations has to be solved self-consistently for the density of every baryon. In model 1 the coupling strength is known *a priori* from the given total baryon density but the rearrangement term in Eq. (32) can only be calculated from Eq. (18) if the composition of the neutron star matter is known. For model 2 the calculation gets even more complex since in addition the strength of the vertices changes with the particle ratios. Furthermore, the rearrangement self-energies of Eq. (22) differ for each baryon multiplet and are strongly affected by the density dependence of the vertices and the density of each particle species. Therefore, one has to include all particles in the calculation and to check for their appearance such that the condition of chemical equilibrium is retained. This leads to a highly nonlinear set of equations where Eqs. (32)-(35) have to be solved self-consistently and the calculation is far more involved than in standard RMF theory.

## B. $\Lambda$ matter

We first study the properties of strange matter for our different choices of the density dependence of the hyperon-meson vertices. This is done by calculating the equation of state for symmetric nuclear matter ( $\rho_p = \rho_n = \frac{1}{2}\rho_N$ ) with a fixed admixture  $f_S$  of  $\Lambda$ -hyperons. The strangeness fraction for  $\Lambda N$  matter is defined as

$$f_S = \frac{\rho_S}{\rho_T} = \frac{\rho_\Lambda}{\rho_N + \rho_\Lambda}. \quad (36)$$

It was pointed out in [40] that  $\Lambda N$  matter will not be the lowest energetic state of strange matter at higher densities and for higher strangeness fractions. A full calculation ensuring chemical equilibrium has to include also the  $\Sigma$  and the  $\Xi$  since the  $\Lambda$  can be converted via non-mesonic decay-channels into these hyperons. But for a systematic study of the effects of the different choices of the scaling factors  $R_{\sigma\Lambda}$  and  $R_{\omega\Lambda}$  for models 1 and 2 we have to restrict ourselves to the admixture of  $\Lambda$ -hyperons since, as discussed in Sec. II C, these are the only hyperons with microscopic derivations for the scaling factors.

In Fig. 1 we show results for the equation of state calculated with the Bonn A parameterization for different strangeness fractions. Comparing within model 1 and 2 the differences

between the set of scaling factors  $R_m$  from microscopic considerations and the set of quark model scaling factors  $R_q$ , one realizes that the equation of state is slightly stiffer in the latter case and that the difference increases with higher densities and higher strangeness fractions. The reason for this is that the reduced strength of the  $\Lambda$  vertices in the microscopic case decreases the potential energy of the hyperons. The softer EoS is also in agreement with the fact that the additional hyperon-hyperon interaction, caused by the  $\sigma_s$  and  $\phi$  mesons and assumed to be strongly attractive at the considered densities [30], is at least in part implicitly included. At first sight this result might be surprising since in both cases  $U_\Lambda^{(N)}$  was adjusted to the same value. But this agreement only exists at saturation density and for very small strangeness fractions. Since the ratio of scalar and vector couplings changes with the density due to their medium-dependence the equations of state differ when leaving the equilibrium density. Strictly, identical EoS were only recovered if scalar and vector potentials scaled proportionally to each other. This is also not the case in a RMF model with constant couplings since the scalar and vector potentials scale differently (partly due to nonlinear interaction terms) but the effect is less pronounced.

For model 1 the minimum of the EoS is shifted to higher densities and bound stronger than in model 2 where the shift of the minima is practically negligible. Overall, the EoS is much softer in model 1 at lower densities and both models approach each other again at higher densities. Here, the behavior of model 2 is in closer agreement with non-relativistic Brueckner calculations where the position of the minimum seems to be shifted to lower densities [35] or is relatively independent of the strangeness fraction [34,36]. However, a comparison with non-relativistic results is difficult since these do not reproduce the correct saturation density of symmetric nuclear matter [50]. This behavior is closer examined in Fig. 2 where we display the saturation density and the binding energy at saturation density as a function of the strangeness fraction. The Groningen parameter set exhibits a less pronounced difference between the different models mainly due to its weaker density dependence at low densities [28]. The differences between model 1 and 2 are always larger than between the different choices  $R_q$  and  $R_m$  of the scaling factors. At high strangeness fractions model 1 and 2 seem to approach each other again. This is obvious since their density dependence is identical in the limit of pure systems. However, the binding energy of pure  $\Lambda$  matter is not identical for model 1 and 2 as can be seen from Fig. 3. The reason is that the scaling factors have been adjusted at  $f_S = 0$  and differ slightly due to the behavior of the vertices at low densities and the different choices of the density dependence. This is seen by comparing the scaling factors of model 1 and 2 in Tab. I. Again, the difference is most pronounced for the Bonn A potential. Results for the DD parameter set are not shown but closely resemble the Groningen results.

This distinct difference is mainly caused by the strong density dependence of the vertices of the Bonn A parameterization at low and very high densities. The reason for this behavior is not the Bonn A potential itself but the polynomial function in  $k_F$  that was used for the parametrization of the self-energies. Even though this function is very accurate around saturation density and well suited for the calculation of finite nuclei [31] it leads to some uncertainties when extrapolated to very low densities. Since in model 2 the hyperon vertizes are adjusted at low densities, where due to numerical difficulties Brueckner calculations are problematic, the extrapolation to higher densities might involve uncertainties. The

extrapolation of model 1 is safe since the hyperon vertices are evaluated around saturation density where they are well defined. The Groningen and the DD parameter sets avoid this problem by choosing a rational function in  $\rho$  to fit the self-energies [45] leading to a stable extrapolation to low and very high densities.

### C. $\beta$ -stable matter

In the following we study the composition of the equation of state for neutron star matter as discussed in Sec. III A. We first examine the case where the vertices depend on the total density (model 1) and consider only  $\Lambda$ -hyperons. This allows us to compare the results with Sec. III B. In Fig. 4 the pressure versus the energy density is shown for the three different interactions. The DD parameter set has the softest EoS, i.e. the lowest pressure at a given  $\epsilon$ , closely followed by the Groningen parameter set while Bonn A is much stiffer at high energy densities. The curves calculated with the scaling factor set  $R_q$  (upper lines) are much stiffer than the curves using the semi-microscopic set  $R_m$  (lower lines). This difference is larger than expected from Figs. 1 and 2. This is mainly due to the reduced repulsive  $\Lambda$ -vector potential for set  $R_m$ . The appearance of the  $\Lambda$  sets in at slightly lower densities which introduces an additional softening of the EoS by a reduction of the kinetic pressure. Remarkably, the differences between the two choices of the scaling factors can be larger than the differences between two parameter sets indicating that a closer examination of the scaling factors  $R_{\alpha\Lambda}$  is necessary. The properties at high energy densities are mainly determined by the density dependence of the vertices. Here, the Groningen and DD parameter set follow closely Brueckner calculations. The high density extrapolation of the Bonn A parameter set leads to an increase of the coupling strength and the contribution from the repulsive  $\omega$  field exceeds the attraction from the  $\sigma$  field causing the stiffer EoS.

For comparison with constant coupling RMF calculations we also performed calculations including the complete baryon octet. The scaling factors  $R_{\alpha Y}$  were determined in the standard approach from SU(6) symmetry (set  $R_q$ , see Table I). Results are shown in Fig. 5. Again, at high densities the Groningen and DD parameter set are much softer than the Bonn A parameter set. But their properties at low and intermediate densities are considerably different. The Groningen EoS exhibits an extreme softening at low densities. This is explained by the early appearance of the  $\Sigma^-$ . The strong coupling to the  $\delta$  field, being only present in the Groningen parameterization, reduces the  $\Sigma^-$  effective mass  $m_{\Sigma^-}^* = M_{\Sigma^-} - \Gamma_{\sigma\Sigma^-}\Phi_\sigma - 2\Gamma_{\delta\Sigma^-}\Phi_\delta$ . In contrast the isoscalar  $\Lambda$  hyperon does not couple to the isovector  $\delta$  meson. Moreover, because of isospin, the effective masses of the  $\Sigma^+$  and  $\Xi^0$  are increased and their thresholds are shifted to higher density regions. This behavior is different from [5] where the inclusion of a constant coupling  $\delta$  meson did not noticeably change the EoS.

Results for the composition of neutron star matter for the different parameter sets are presented in Fig. 6. One recognizes that the early and strong appearance of the  $\Sigma^-$  temporarily reduces the electron fraction and strongly suppresses the myons. Clearly, this behavior opposes other results of RMF and Brueckner calculations, e.g. [5,7]. The extraction of the isovector couplings from the Groningen potential leads to relatively large values indicating a slight increase of the  $\delta$  coupling above saturation density. This might cause the observed

behavior and could be fixed by adjusting the scaling factor  $R_{\delta\Sigma^-}$  to the strength of the  $\Sigma$  isovector potential. Since experimental data is not available we used  $R_{\Sigma\delta} = R_{\rho\Sigma} = 2$  from SU(6) symmetry instead. Further investigations are necessary.

The composition of neutron star matter for the DD parameter set resembles the outcome of non-relativistic Brueckner calculations [6,7] with the  $\Sigma^-$  appearing before the  $\Lambda$ . For the Bonn A parameter set the  $\Lambda$  and  $\Sigma^-$  appear at relatively high densities of about  $2.5 - 3\rho_0$  which also explains the stiffer equation of state. At higher densities when the other hyperons are present the number of hyperons exceeds the number of neutrons. This behavior is observed for all parameter sets with the strongest effect for the Groningen parameter set. The same result was also found in other models, e.g. [2,5].

As mentioned in Sec. I one problem of RMF calculations with coupling constants fitted to properties of finite nuclei is the appearance of negative effective masses in neutron star matter at densities of  $\rho \approx 0.5 - 1 \text{ fm}^{-3}$  [5]. This is mainly caused by the small effective mass at saturation density that is needed in order to reproduce the observed spin-orbit splitting in finite nuclei [18]. This causes a rather stiff equation of state and confirms that the extrapolation of phenomenological parameter sets to high densities can be problematic. In the DDRH approach negative effective masses appear only at much higher densities where the validity of the model is already questionable because baryons and mesons will cease to be the relevant degrees of freedom. We therefore stop the calculation when negative effective masses appear and do not attempt to extrapolate to higher densities as in [5,22]. For the Bonn A parameter set  $m^*$  gets negative around  $\rho \approx 1 - 1.2 \text{ fm}^{-3} \approx 6 - 8\rho_0$  being mainly caused by the mentioned increase of the  $\sigma$  coupling strength at high densities. For the Groningen parameter set the neutron effective mass gets negative at around  $\rho \approx 1.2 \text{ fm}^{-3}$ . The reason is here the additional reduction of  $m_n^*$  by the coupling to the  $\delta$  meson. For the DD parameter set  $m^*$  is still positive for the highest considered densities of  $\rho = 1.5 \text{ fm}^{-3}$ . The different behavior of the DDRH model compared to constant coupling models originates in the density dependence of the vertices and is mainly caused by the fact that the vertex density dependence takes into account information from wider density range as found in finite nuclei and allows a safer extrapolation to higher densities. The medium dependence of the vertices implicitly includes higher order correction terms that can be partly identified with the nonlinear meson self-interactions of RMF models. Also, this explains why models with nonlinear vector self- interactions [19,20] follow more closely DB calculations avoiding negative effective masses.

Finally, we turn to the discussion of the results obtained with model 2. In Fig. 7 the equation of state for the different density dependent interactions is shown and Fig. 8 displays the corresponding particle distributions. Compared to model 1 the hyperons appear at very high densities of about  $3\rho_0$ . In addition their ratio increases very fast and around  $3 - 4\rho_0$  the number of  $\Lambda$ s already exceeds the number of neutrons. This leads to a stiffer EoS at low densities and a strong softening above  $\epsilon = 500 \text{ MeV fm}^{-3}$ . The suppression of the hyperons in model 2 is a direct consequence of the different choice of the density dependence. The different rearrangement self-energies for each baryon multiplet induce a relative shift in the chemical potentials that impedes the appearance of the hyperons. The differences between the choices of scaling factors  $R_{\alpha\Lambda}$  are the least pronounced for the Bonn A parameter set having the strongest density dependence and the most pronounced for the DD parameter set having the weakest density dependence. Here, the  $\Lambda$  does not appear for the densities

considered if the scaling factor set  $R_q$  is chosen. This leads to the stiffest equation of state. For the semi-microscopic set  $R_m$  all interactions have very similar equations of state approaching asymptotically the results of model 1 at high densities. Using set  $R_q$  from SU(6) symmetry and including all octet hyperons we found that the appearance of the  $\Sigma$  and the  $\Xi$  is shifted to even higher densities ( $\rho > 0.7 \text{ fm}^{-3}$ ) or is completely suppressed for all interactions and does not noticeably modify the EoS.

We conclude that the composition of neutron star matter strongly depends on the density dependence of the interaction. In practice this is problematic in model 2 since the low density behavior of the vertices has to be extrapolated from DB calculations and introduces additional uncertainties. On the other hand, there are indications that model 2 resembles the outcome of Brueckner calculations. Improvements of DB calculations in the low density region might resolve these problems. Again, we remark that we expect that a realistic density dependence is a mixture of model 1 and 2 and has to be determined from DB calculations of strange matter.

#### IV. NEUTRON STARS

The condition of hydrodynamical equilibrium inside a neutron star determines the connection between experimentally observable properties like the mass and possibly the radius of a neutron star and the theoretical equation of state of neutron star matter. In this work we only consider static spherically symmetric neutron stars. The condition of hydrodynamical equilibrium in general relativity is expressed by the Tolman-Oppenheimer-Volkoff (TOV) differential equations [51]

$$\frac{dm(r)}{dr} = 4\pi r^2 \epsilon(r) \quad (37)$$

$$\frac{dP(r)}{dr} = -\frac{[\epsilon(r) + P(r)][m(r) + 4\pi P(r)r^3]}{r^2 \left[1 - \frac{2m(r)}{r}\right]}, \quad (38)$$

where  $r$  is the radial distance from the origin of the neutron star and  $m(r)$  is the mass contained in a sphere of radius  $r$  inside the star. The gravitational constant  $G$  has been set to 1 for simplicity. Pressure  $P(r)$ , energy  $\epsilon(r)$  and mass  $m(r)$  distributions can be calculated for a given pressure-energy relation  $P(\epsilon)$  as discussed in section III. The differential equations are solved by integrating from the center, starting with a central pressure  $P_c$ , until the surface (radius  $r = R$ ,  $P(R) = 0$ ) of the neutron star is reached. The radius  $R$  of the star and its gravitational mass are related by  $M = m(R) = 4\pi \int_0^R dr r^2 \epsilon(r)$ . Varying the central pressure one finds a mass-radius relation  $M(R)$  describing a family of neutron stars that will depend on the choice of the equation of state.

Since it is a well known fact that Brueckner theory breaks down at very low densities one cannot rely solely on an EoS derived from the  $NN$  interaction for the description of neutron stars. Furthermore, in the surface region of neutron stars a so called crust of sub-nuclear density (where  $\rho$  is much lower than the normal nuclear matter saturation density  $\rho_0$ ) exists consisting of atoms and nuclei and having its own specific degrees of freedom. Even though the crust contributes only about 1% to the total mass and does not strongly

affect the maximum mass of the star, its thickness is about 10% of the radius and influences the size of very light stars.

For the above reasons, we use the Baym-Pethick-Sutherland (BPS) EoS [52] for sub-nuclear densities  $\rho < 0.001 \text{ fm}^{-3}$  and results of Negele and Vautherin for densities of  $\rho > 0.001 \text{ fm}^{-3}$  [53]. The transition density to the DDRH EoS is defined by the intersection of both EoS. One finds values between  $0.3 \rho_0$  and  $0.7 \rho_0$  depending on the different interactions.

In Fig. 9 mass-radius relations calculated with the equation of state of the Groningen parameter set are shown. For model 1 we find maximum masses of  $M_{\max} = 1.69M_{\odot}$  for the semi-microscopic scaling factor set  $R_m$  and  $M_{\max} = 1.89M_{\odot}$  for the SU(6) set  $R_q$ . Including the full set of octet hyperons into the EoS the mass is further reduced to  $M_{\max} = 1.65M_{\odot}$ . The maximum density in the center of the star is similar in all three models and reaches  $\rho_c \simeq 0.91 - 0.99 \text{ fm}^{-3}$  which corresponds to  $5 - 6\rho_0$ . Including all hyperons the minimum radius of the neutron star decreases from  $R_{\min} \simeq 11.7 \text{ km}$  to  $R_{\min} \simeq 10.8 \text{ km}$  and the radius of neutron stars with the typical experimentally observed mass of  $M = 1.4M_{\odot}$  is reduced from  $R = 12.7 \text{ km}$  to  $R = 11.7 \text{ km}$ . The smaller radii are caused by the early occurrence of the  $\Sigma^-$  and the softening of the EoS at low densities that was discussed in Sec. III C. Also, the star mainly consists of hyperons as can be seen from the particle composition of Fig. 6. Model 2 leads to significantly higher maximum masses of  $M_{\max} = 1.95M_{\odot}$  ( $R_m$ ) respectively  $M_{\max} = 2.12M_{\odot}$  ( $R_q$ ) because of the appearance of the hyperons only at higher densities. Since, in addition, the maximum central density is only about  $\rho_c \simeq 0.73 \text{ fm}^{-3}$  the star is mainly composed of nucleons.

From these results the density dependence of model 1 seems to be favored because of the closer agreement with other calculations of neutron star masses. The big difference between the maximum masses for the two sets  $R_q$  resp.  $R_m$  emphasizes the sensitivity of the model to the choice of the scaling factors  $R_{\alpha Y}$ . The effect is as large as the inclusion of additional hyperons and should also be examined in RMF calculations with density independent coupling constants.

For the Bonn A parameter set we find comparable results as is seen from Fig. 10. The maximum masses for model 1 of  $M_{\max} = 1.76M_{\odot}$  ( $R_m$ ) resp.  $M_{\max} = 2.07M_{\odot}$  ( $R_q$ ) (only  $\Lambda$ ) and the central density  $\rho_c \simeq 1.15 \text{ fm}^{-3}$  are higher than for the Groningen parameter set due to the stiffer equation of state. Including the full set of octet hyperons the maximum mass is not reached before the effective mass gets negative at about  $\rho \simeq 1.02 \text{ fm}^{-3}$  where a mass of  $M = 1.81M_{\odot}$  is found. The same is observed for model 2 where the effective mass gets negative at about the same density indicating maximum masses higher than  $1.7M_{\odot}$  ( $R_m$ ) resp.  $1.8M_{\odot}$  ( $R_q$ ). Despite these differences the radii of neutron stars with  $1.4M_{\odot}$  are all in the range of  $R = 12.5 - 12.8 \text{ km}$  and in close agreement with the results for the Groningen parameter set.

Results for the DD parameter set are displayed in Fig. 11. Having the softest equation of state at high densities, this interaction also exhibits the smallest maximum masses of  $M_{\max} = 1.43M_{\odot}$  ( $R_m$ ) resp.  $M_{\max} = 1.66M_{\odot}$  ( $R_q$ ) (Model 1, only  $\Lambda$ ) and  $M_{\max} = 1.44M_{\odot}$  (Model 1, all hyperons). For model 2 the masses are again higher ( $M_{\max} = 1.77M_{\odot}$  resp.  $M_{\max} = 2.08M_{\odot}$ ) since the stars are mainly composed of nucleons. The DD parameter set reaches central densities up to  $\rho_c \simeq 1.3 \text{ fm}^{-3}$  in model 1 and  $\rho_c \simeq 1.0 \text{ fm}^{-3}$  in model 2. The soft equation of state reduces also the radius of the neutron stars. One finds a minimum radius of  $R_{\min} \simeq 10.3 \text{ km}$  and a radius of  $R \simeq 10.8 \text{ km}$  for a mass of  $1.4M_{\odot}$  if all hyperons

are included.

Even though the three different parameter sets and the different choices of the density dependence give different predictions for the maximum mass of a neutron star the radius of a typical neutron star with a mass of  $M = 1.4M_{\odot}$  is in all models expected to be about 12.5 km while the minimum radius can get as small as 10.3 km. This is explained by the fact that the radii are mainly influenced by the low to intermediate density behavior of the EoS which is similar in all considered models. On the other hand, the maximum masses are strongly influenced by the high density behavior being quite different for the investigated interactions and models 1 and 2. Our results are compatible with non-relativistic Brueckner calculations [6,7,54] and relativistic Hartree-Fock calculations (fitted to the Bonn A NN potential) [22] that predict radii of 10–12 km and also possess a rather soft equation of state. In contrast, most relativistic mean-field models with density independent coupling constants find radii of 13–15 km, e.g. [2,55]. Our maximum neutron star masses of  $1.44 - 1.8M_{\odot}$  agree with the outcome of different RMF calculations while non-relativistic Brueckner calculations favor values of  $\sim 1.3M_{\odot}$ . This indicates that the non-relativistic EoS might be too soft at higher densities where relativistic effects become more important. The high value of  $\sim 1.8M_{\odot}$  found for the Bonn A potential is probably caused by the inaccuracies from the polynomial extrapolation of the density dependent vertices to the high density region. Therefore, we favor the results of the Groningen and DD parameter set. We also performed calculations with a purely hadronic EoS to examine the total effect of the hyperons on the EoS. For the DD interaction a maximum mass of  $2.05M_{\odot}$  was found while the Groningen and Bonn A parameter sets have masses of  $2.35M_{\odot}$  resp.  $2.45M_{\odot}$ . The observed reduction  $\Delta M \sim 0.5 - 0.7M_{\odot}$  of the maximum mass caused by the inclusion of the hyperons is comparable to other models [1,6,7].

## V. SUMMARY AND CONCLUSION

We have extended the DDRH model to the strangeness sector including the full set of  $SU(3)_f$  octet baryons. Using realistic density dependent interactions derived from DB calculations we examined the properties of neutron star matter. Starting with a medium-dependent NN interaction that is parameterized by density dependent meson-nucleon vertices we found that the extension of DB results from nuclear matter to hypermatter is not unique. The structure of the DB interaction strongly indicates that the ratio  $R_{\alpha Y}$  of the nucleon and hyperon in- medium vertices and self-energies is mainly determined by the ratio of the corresponding free-space coupling constants and is only weakly affected by the background medium. We developed two different models to describe the connection of the density dependence of the baryon vertices to the surrounding medium. In model 1 the vertices depend on the total baryon density and are not influenced by the strangeness asymmetry of the medium. This ensures that the relative strength of the vertices remains constant and follows closely the behavior of RMF calculations with constant couplings. An extreme assumption in this model is that the vertices are influenced equally from all baryons. However, in first order hyperons and nucleons should be independent of each other. This was investigated in model 2 that assumes a dependence of the vertices only on the baryons within the corresponding  $SU(3)_f$  multiplet. While this leads to a more realistic description

of slightly asymmetric systems, the model becomes problematic at very high asymmetries since it completely neglects the higher order effects from of the other baryon multiplets. In addition, in such systems the low density behavior turns out to be important which is not well determined from Brueckner calculations. We examined the properties of  $N\Lambda$  matter and found differences between the two models mainly at low densities and strangeness fractions  $f_S$  that are nearly vanishing at high densities and values of  $f_S$  close to one. The conclusion is that a realistic medium dependence of the in- medium vertices should be a mixture of both models including the asymmetry and the total density. Such a description is pending until DB calculations for the full strangeness octet will be available.

Application of the DDRH theory to weak  $\beta$ -stable matter leads to more complex condition for chemical equilibrium than in mean-field calculations with constant coupling constants. The occurrence of rearrangement contributions to the chemical potential connects all particle densities strongly to each other which complicates the practical calculation considerably.

An important aspect in our calculations is the value of the scaling factors  $R_{\alpha Y}$ . Microscopic calculations of the  $\sigma\Lambda$  vertex show a strong deviation from the quark model value. Choosing either  $R_{\sigma\Lambda} = 0.49$  from  $N\Lambda$  T-matrix results (scaling factor set  $R_m$ ) or  $R_{\omega\Lambda} = 2/3$  from SU(6) symmetry considerations (set  $R_q$ ) and fixing the remaining scaling factors to the same experimental potential depth of the  $\Lambda$  we found strong differences in the equation of state. The smaller microscopic values lead to a much softer EoS and reduce the calculated maximum neutron star masses by 10-15%. This behavior even though enhanced by the density dependence of the interaction will also be visible for parameter sets with density independent coupling constants and should be closely examined. Microscopic calculations for the  $\Sigma$  and  $\Xi$  vertices are not available restricting full scale neutron star calculations to the SU(6) symmetry values. But one has to review if these values are realistic and study effects of their modification on neutron star properties [56,57].

We remark that our calculations did not examine the influence of the hidden- strangeness mesons  $\sigma_s$  and  $\phi$  explicitly that are assumed to cause a highly attractive hyperon-hyperon interaction at intermediate densities and might lead to a small reduction of the neutron star radii. On the other hand, the couplings of these mesons posses some uncertainties that cannot be reliably fixed since experimental data are missing. In addition they are in part implicitly included in the microscopic scaling factors.

An examination of neutron star properties favors model 1 as choice for highly asymmetric dense systems. While model 2 predicts too high maximum masses and a suppression of the hyperons, the results for model 1 are in close agreement with other calculations. For all examined density dependent interactions we find radii of  $10 - 13$  km for neutron stars with masses above  $1.4M_\odot$ . This is also observed in non-relativistic Brueckner calculations while RMF calculations with phenomenological interactions usually favor larger radii. Our maximum masses of  $M_{\max} = 1.65M_\odot$  for the Groningen parameter set and  $M_{\max} = 1.44M_\odot$  for the DD parameter set are confirmed by other RMF calculations and are slightly higher than in Brueckner calculations.

We conclude that the DDRH model allows a consistent calculation of strange matter and neutron stars and yields results that are comparable with other models. It incorporates the properties of the DB model using microscopic interactions at various densities as input. The extrapolation to higher densities is more constrained than for phenomenological RMF

calculations that use only information from the limited density range of finite nuclei for the determination of their parameters. Improvements of the results, a more realistic density dependence of the hyperon-meson vertices and more restricted predictions will be possible if results from upcoming DB calculations for the  $SU(3)_f$  baryon octet are available.

#### **ACKNOWLEDGEMENT**

We would like to thank C. Greiner and K. Schertler for interesting discussions and helpful comments. This work was supported in part by DFG (Contract No. Le439/4-3), GSI Darmstadt, and BMBF.

## REFERENCES

- [1] S. Balberg and A. Gal, Nucl. Phys. **A625**, 435 (1997); S. Balberg, I. Lichtenstadt and G. B. Cook, Apl. J. Suppl. **121**, 515 (1999).
- [2] N. K. Glendenning, Phys. Lett. **B114**, 392 (1982); N. K. Glendenning, Astrophys. J. **293**, 470 (1985); N. K. Glendenning, Z. Phys. **A327**, 295 (1987).
- [3] F. Weber and M. K. Weigel, J. Phys. **G15**, 765 (1989).
- [4] R. Knorren, M. Prakash and P. J. Ellis, Phys. Rev. **C52**, 3470 (1995).
- [5] J. Schaffner and I. N. Mishustin, Phys. Rev. **C53**, 1416 (1996);
- [6] M. Baldo, G. F. Burgio, H. J. Schulze, Phys. Rev. **C61**, 055801 (2000).
- [7] I. Vidana, A. Polls, A. Ramos, L. Engvik and M. Hjorth-Jensen, nucl-th/0004031.
- [8] H. Hanauske, D. Zschiesche, S. Pal, S. Schramm, H. Stocker and W. Greiner, Astrophys. J. **537**, 50320 (2000).
- [9] S. Pal, M. Hanauske, I. Zakout, H. Stocker and W. Greiner, Phys. Rev. **C60**, 015802 (1999).
- [10] H. Muether, M. Prakash and T. L. Ainsworth, Phys. Lett. **199**, 469 (1987).
- [11] L. Engvik, M. Hjorth-Jensen, E. Osnes, G. Bao and E. Ostgaard, Phys. Rev. Lett. **73**, 2650 (1994).
- [12] J. D. Walecka, Annals Phys. **83**, 491 (1974).
- [13] B. D. Serot and J. D. Walecka, Adv. Nucl. Phys. **16**, 1 (1986).
- [14] M. Rufa, H. Stoecker, P. G. Reinhard, J. Maruhn und W. Greiner, J. Phys. **G13**, L143 (1987).
- [15] J. Mares und J. Zofka, Z. Phys. **A333**, 209 (1989).
- [16] M. Rufa, J. Schaffner, J. Maruhn, H. Stoecker, W. Greiner und P. G. Reinhard, Phys. Rev. **C42**, 2469 (1990).
- [17] N. K. Glendenning, D. Von-Eiff, M. Haft, H. Lenske und M. K. Weigel, Phys. Rev. **C48**, 889 (1993)
- [18] P. G. Reinhard, Z. Phys. **A329**, 257 (1988).
- [19] A. R. Bodmer, Nucl. Phys. **A526**, 703 (1991).
- [20] Y. Sugahara, H. Toki, Nucl. Phys. **A579**, 557 (1994).
- [21] F. Weber and M. K. Weigel, Nucl. Phys. **A505**, 779 (1989).
- [22] H. Huber, F. Weber, M. K. Weigel and C. Schaab, Int. J. Mod. Phys. **E7**, 301 (1998).
- [23] R. Brockmann, H. Toki, Phys. Rev. Lett. **68**, 3408 (1992).
- [24] H. Lenske and C. Fuchs, Phys. Lett. **B345**, 355 (1995).
- [25] C. Fuchs, H. Lenske and H. H. Wolter, Phys. Rev. **C52**, 3043 (1995).
- [26] F. Ineichen, M. K. Weigel, D. Von-Eiff Phys. Rev. **C53**, 2158 (1996).
- [27] M. L. Cescato, P. Ring, Phys. Rev. **C57**, 134 (1998).
- [28] F. Hofmann, C. M. Keil, H. Lenske, nucl-th/0007xxx.
- [29] C. M. Keil, F. Hofmann and H. Lenske, Phys. Rev. **C61**, 064309 (2000).
- [30] J. Schaffner, C. B. Dover, A. Gal, C. Greiner, D. J. Millener and H. Stocker, Annals Phys. **235**, 35 (1994).
- [31] S. Haddad, M. Weigel, Phys. Rev. **C48**, 2740 (1993).
- [32] F. de Jong and H. Lenske, Phys. Rev. **C57**, 3099 (1998).
- [33] J.W. Negele, Rev. Mod. Phys. **54**, 913 (1982).

- [34] H. J. Schulze, M. Baldo, U. Lombardo, J. Cugnon and A. Lejeune, Phys. Rev. **C57**, 704 (1998).
- [35] V. G. Stoks and T. S. Lee, Phys. Rev. **C60**, 024006 (1999).
- [36] I. Vidana, A. Polls, A. Ramos, M. Hjorth-Jensen and V. G. Stoks, Phys. Rev. **C61**, 025802 (2000).
- [37] C. B. Dover and A. Gal, Prog. Part. Nucl. Phys. **12**, 171 (1985).
- [38] C. B. Dover, D. J. Millener and A. Gal, Phys. Rept. **184**, 1 (1989).
- [39] J. Mares, E. Friedman, A. Gal and B. K. Jennings, Nucl. Phys. **A594**, 311 (1995)
- [40] J. Schaffner-Bielich and A. Gal, nucl-th/0005060.
- [41] R. Brockmann and R. Machleidt, Phys. Rev. **C42**, 1965 (1990).
- [42] R. Machleidt, Adv. Nucl. Phys. **19**, 189 (1989).
- [43] F. de Jong and H. Lenske, Phys. Rev. **C58**, 890 (1998)
- [44] R. Malfliet, Prog. Part. Nucl. Phys. **21**, 207 (1988).
- [45] S. Typel and H. H. Wolter, Nucl. Phys. **A656**, 331 (1999).
- [46] A. Reuber, K. Holinde, H. C. Kim and J. Speth, Nucl. Phys. **A608**, 243 (1996)
- [47] J. Haidenbauer, W. Melnitchouk and J. Speth, Proceedings of SENDAI 98, nucl-th/9805014.
- [48] Z. Ma, J. Speth, S. Krewald, B. Chen and A. Reuber, Nucl. Phys. **A608**, 305 (1996).
- [49] N. M. Hugenholtz and L. van Hove, Physica **24**, 363 (1958).
- [50] F. Coester, S. Cohen, B. D. Day and C. M. Vincent, Phys. Rev. **C1**, 769 (1970).
- [51] J. R. Oppenheimer and G. M. Volkoff, Phys. Rev. **55**, 374 (1939).
- [52] G. Baym, C. Pethick and P. Sutherland, Astrophys. J. **170**, 299 (1971).
- [53] J. Negele and D. Vautherin, Nucl. Phys. **A207**, 298 (1973).
- [54] A. Akmal, V. R. Pandharipande and D. G. Ravenhall Phys. Rev. **C58**, 1804 (1998).
- [55] K. Schertler, C. Greiner, J. Schaffner-Bielich and M. H. Thoma, astro-ph/0001467.
- [56] N. K. Glendenning and S. A. Moszkowski, Phys. Rev. Lett. **67**, 2414 (1991).
- [57] H. Huber, M. K. Weigel and F. Weber, Z. Naturforsch. **54A**, 77 (1999).

## FIGURES

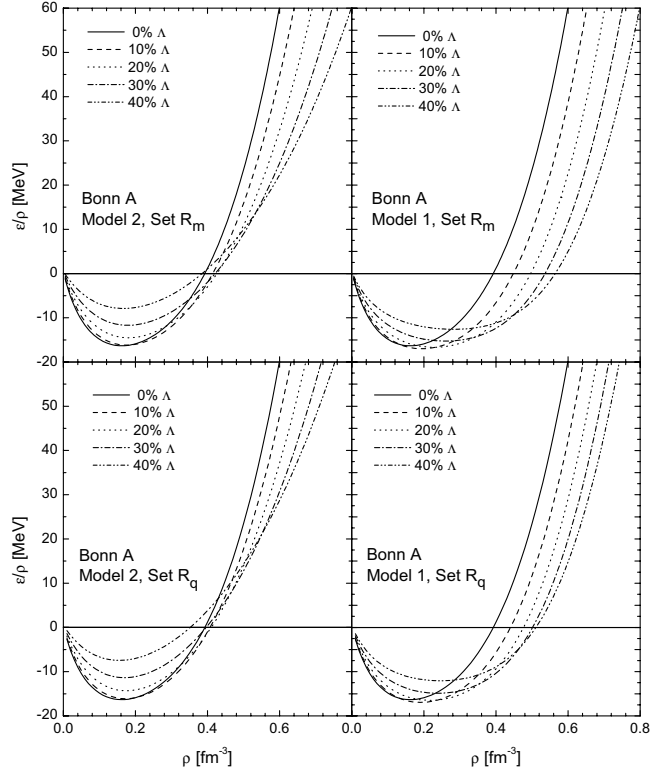


FIG. 1. Equation of state of symmetric nuclear matter for  $\Lambda$  admixtures from 0% to 40%. Shown are results for the Bonn A NN potential for different choices of the density dependence (model 1 and 2) and the scaling factors (set  $R_q$  and  $R_m$ ) .

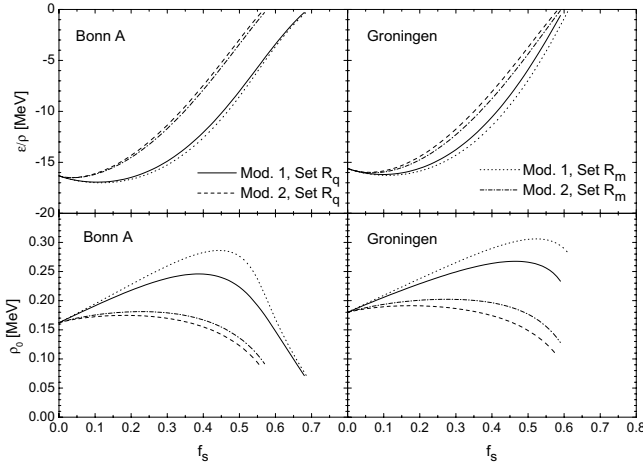


FIG. 2. Binding energy (top) and saturation density (bottom) as a function of the strangeness fraction  $f_s$  for the different choices of the  $\Lambda$  vertex. Results are shown for the Bonn A (left) and the Groningen (right) parameter set.

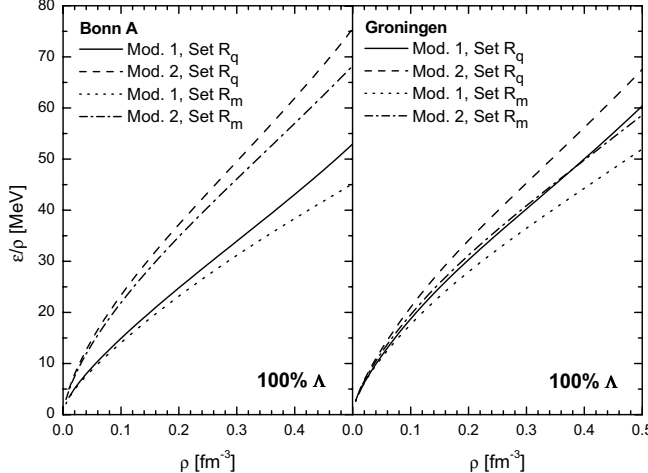


FIG. 3. Binding energy of pure  $\Lambda$  matter as a function of the density for the different choices of the  $\Lambda$  vertex. Results are shown for the Bonn A (left) and the Groningen (right) parameter set.

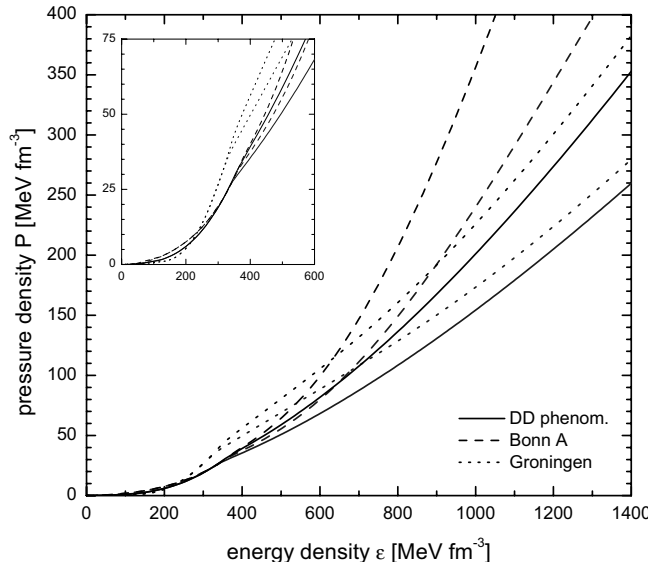


FIG. 4. Equation of state for neutron star matter in the DDRH model for different density dependent interactions. Results are shown for model 1 including only the  $\Lambda$  and the different scaling factors. The upper line of each interaction corresponds to calculations with set  $R_q$  and the lower one to calculations with set  $R_m$ . For details see text.

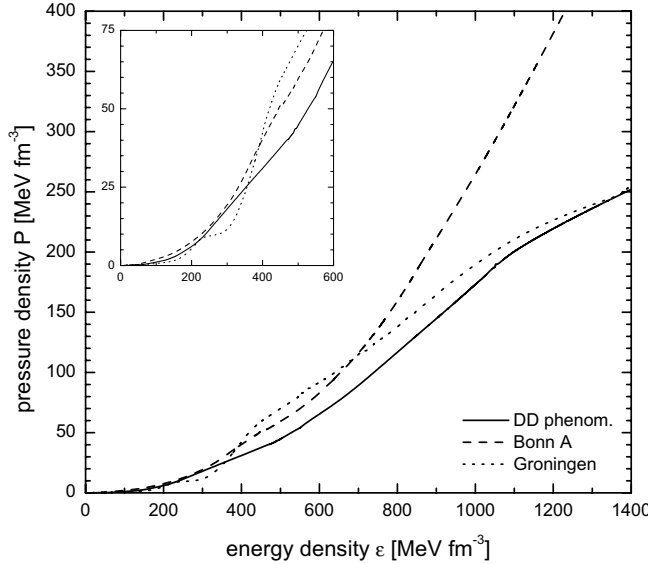


FIG. 5. Equation of state for neutron star matter for model 1 including all hyperons. Results are shown for the phenomenological density dependence of Ref. [45] (solid line), Groningen parameter set (dotted line) and Bonn A parameter set (dashed line). The SU(6) scaling factors from set  $R_q$  are used.

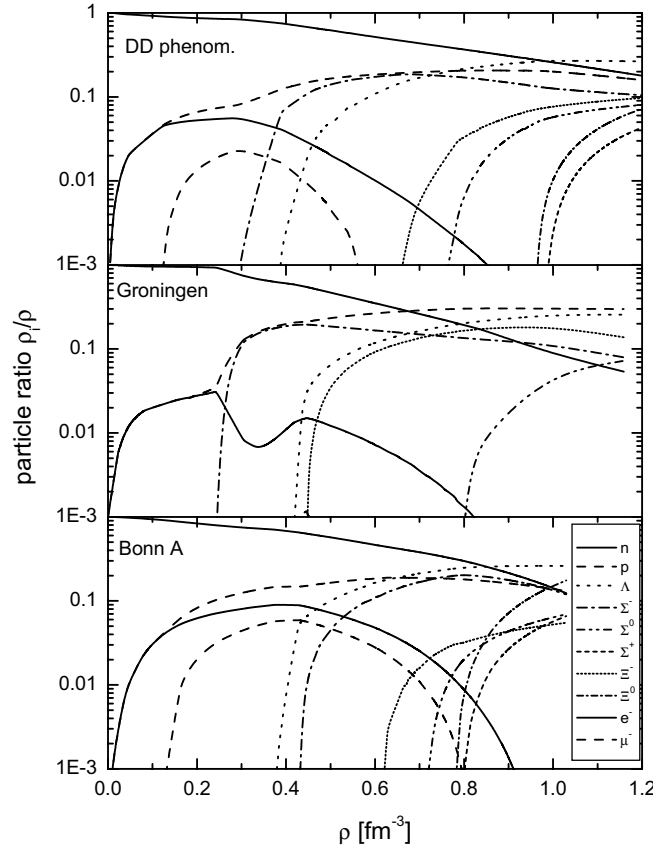


FIG. 6. Composition of  $\beta$ -stable matter in the DDRH model for the phenomenological density dependence of Ref. [45] (top), Groningen parameter set (middle) and Bonn A parameter set (bottom). Results are shown for model 1 including all hyperons and scaling factor set  $R_q$ .

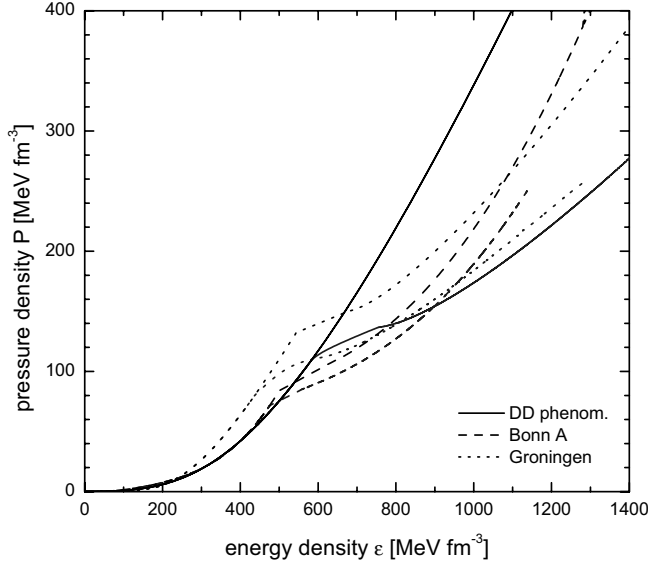


FIG. 7. Same as Fig. 4, but results are shown for model 2.

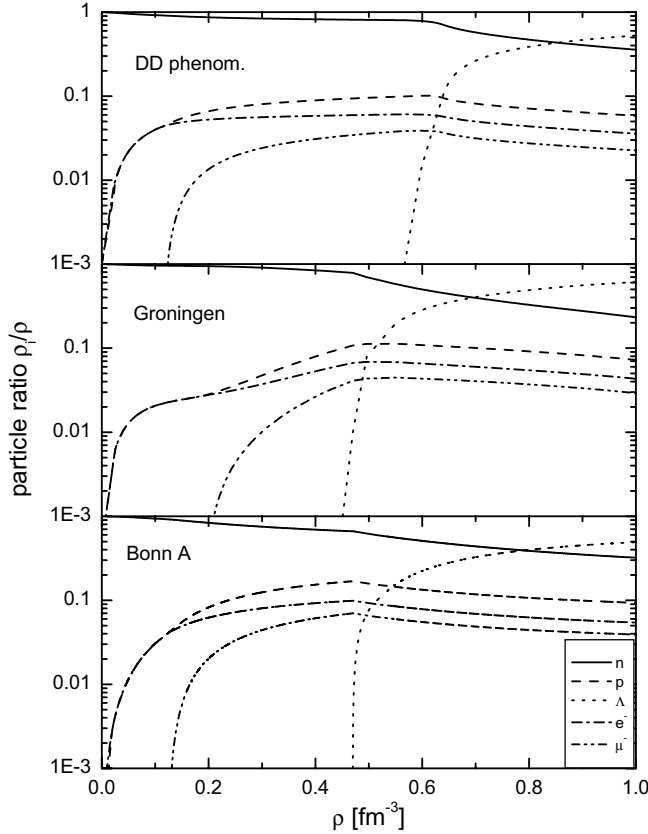


FIG. 8. Same as Fig. 6, but the density dependence is implemented with model 2. The scaling factor set  $R_m$  was used.

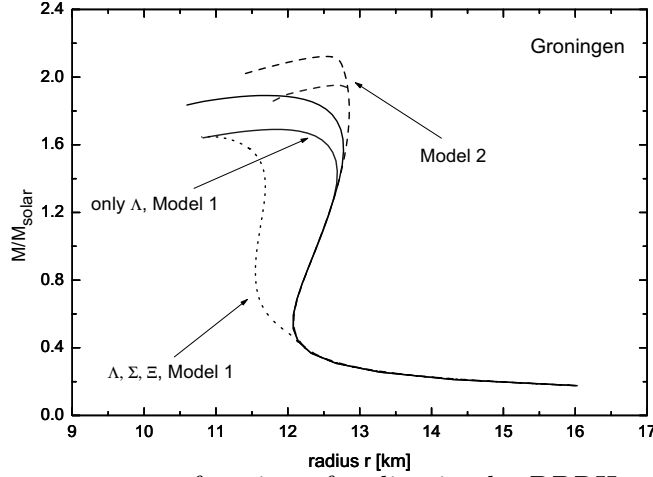


FIG. 9. Neutron star mass as a function of radius in the DDRH model for the Groningen parameter set. Results for model 1 including only  $\Lambda$  (solid lines), model 1 including all hyperons (dotted lines) and model 2 (dashed lines) are compared. The upper line of each model corresponds to calculations with set  $R_q$  the lower one to calculations with set  $R_m$ . For details see text.

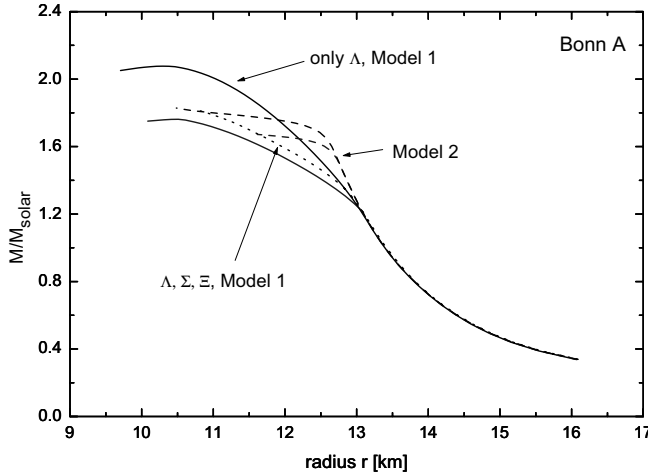


FIG. 10. Same as Fig. 9 but for the Bonn A parameter set.

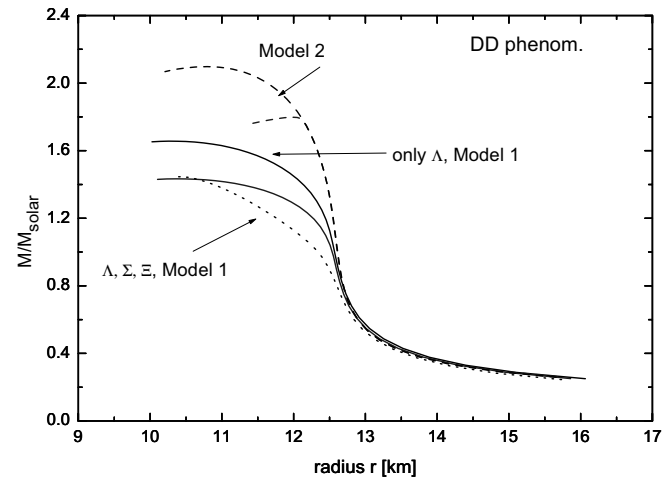


FIG. 11. Same as Fig. 9 but for the phenomenological density dependence of Ref. [45].

## TABLES

	$R_m$		$R_q$			
	$R_{\sigma\Lambda}$	$R_{\omega\Lambda}$	$R_{\sigma\Lambda,\Sigma}$	$R_{\omega\Lambda,\Sigma}$	$R_{\sigma\Xi}$	$R_{\omega\Xi}$
model 1						
Bonn A	0.49	0.4935	0.6225	2/3	0.3618	1/3
Groningen	0.49	0.5217	0.6061	2/3	0.3343	1/3
DD phenom.	0.49	0.5100	0.6170	2/3	0.3421	1/3
	$R_m$		$R_q$			
	$R_{\sigma\Lambda}$	$R_{\omega\Lambda}$	$R_{\sigma\Lambda,\Sigma}$	$R_{\omega\Lambda,\Sigma}$	$R_{\sigma\Xi}$	$R_{\omega\Xi}$
model 2						
Bonn A	0.49	0.5690	0.5690	2/3	0.3040	1/3
Groningen	0.49	0.5387	0.5921	2/3	0.3222	1/3
DD phenom.	0.49	0.5251	0.6061	2/3	0.3287	1/3

TABLE I. Scaling factor sets  $R_q$  and  $R_m$  for the  $\sigma$  and  $\omega$  hyperon-meson vertices of model 1 and 2. For details see text.